

RESEARCH ARTICLE

Discovering Hominins - Application of Medical Computed Tomography (CT) to Fossil-Bearing Rocks from the Site of Malapa, South Africa

Jacqueline S. Smilg^{1,2*}, Lee R. Berger^{2,3}

1 Department of Diagnostic Radiology, Charlotte Maxeke Johannesburg Academic Hospital, Johannesburg, South Africa, **2** Evolutionary Studies Institute, University of the Witwatersrand, Johannesburg, South Africa, **3** Department of Science and Technology/National Research Foundation Centre of Excellence in Palaeosciences, University of the Witwatersrand, Johannesburg, South Africa

* jsmilg@yahoo.com



Abstract

In the South African context, computed tomography (CT) has been used applied to individually prepared fossils and small rocks containing fossils, but has not been utilized on large breccia blocks as a means of discovering fossils, and particularly fossil hominins. Previous attempts at CT imaging of rocks from other South African sites for this purpose yielded disappointing results. For this study, 109 fossil-bearing rocks from the site of Malapa, South Africa were scanned with medical CT prior to manual preparation. The resultant images were assessed for accuracy of fossil identification and characterization against the standard of manual preparation. The accurate identification of fossils, including those of early hominins, that were not visible on the surface of individual blocks, is shown to be possible. The discovery of unexpected fossils is reduced, thus lowering the potential that fossils could be damaged through accidental encounter during routine preparation, or even entirely missed. This study should significantly change the way fossil discovery, recovery and preparation is done in the South African context and has potential for application in other palaeontological situations. Medical CT imaging is shown to be reliable, readily available, cost effective and accurate in finding fossils within matrix conglomerates. Improvements in CT equipment and in CT image quality are such that medical CT is now a viable imaging modality for this palaeontological application.

OPEN ACCESS

Citation: Smilg JS, Berger LR (2015) Discovering Hominins - Application of Medical Computed Tomography (CT) to Fossil-Bearing Rocks from the Site of Malapa, South Africa. PLoS ONE 10(12): e0145340. doi:10.1371/journal.pone.0145340

Editor: Michael D. Petraglia, University of Oxford, UNITED KINGDOM

Received: September 30, 2015

Accepted: December 2, 2015

Published: December 18, 2015

Copyright: © 2015 Smilg, Berger. This is an open access article distributed under the terms of the [Creative Commons Attribution License](https://creativecommons.org/licenses/by/4.0/), which permits unrestricted use, distribution, and reproduction in any medium, provided the original author and source are credited.

Data Availability Statement: All relevant data are within the paper.

Funding: The authors have no support or funding to report.

Competing Interests: The authors have declared that no competing interests exist.

Introduction

Fossils offer tangible evidence of the past and are important for the study of the prehistory of life on Earth. They are typically formed through diagenesis and object replacement by a wide variety of minerals and elements [1]. In the Cradle of Humankind (COH) World Heritage site [2], fossils from the Plio-Pleistocene era are usually found in dolomitic limestone caves,

encased in hard calcified sediments. These are often referred to as breccias or calcified clastic matrix [1,3]. This breccia encases bones and varies in its hardness and density. Whilst the strength of the rock has protected the fossils, the density of the rock also makes extraction of the fossils from their surrounding matrix difficult.

Traditionally fossils have been manually prepared from their encasing matrix, or prepared using methods involving acetic or other acids. This involves both mechanical or chemical extraction which is often time consuming and potentially damaging to the fossils themselves [3]. Furthermore, the search for fossils immediately below the surface of the rock being prepared (beyond those made visible by the extraction process or by natural erosion), is typically a haphazard affair, traditionally completely reliant upon the skills of the preparator and random chance. It is therefore often very difficult to completely clean or reconstruct fossils without in some way damaging them. Compounding the difficulty of preparation, fossils are also often incomplete or filled with calcified matrix [4]. These manual methods of preparation are, in addition, destructive to the surrounding matrix and information not recognized during the process may be permanently lost. Even advances in preparation using automated techniques suffer these same problems [5]. Traditional methods of fossil preparation often severely limit research and due to the fact that many fossils of interest to palaeontologists are exceedingly rare, other methods have been examined to allow better visualization and interpretation, whilst at the same time potentially preserving the fossil material and associated matrix. Advances in computer technology, software and the quality of X-rays machines have seen an increase in the use of these X-ray based modalities to “virtually” prepare fossils [6]

X-rays have been commonly used for medical diagnosis since their discovery in 1895 by Wilhelm Röntgen. The use of X-rays in palaeontology dates back to 1896, when Brühl [7] in Berlin and Lemoine [8] in Paris first used X-rays to image fossils. Branco [9] produced the first published work on the use of X-rays for fossil imaging in 1906, followed by Jaekel in 1921, Mautz in 1929 and Lehmann in 1934, who investigated the marine fossils of the Hünseruck slate with X-ray images [9]. Wilhelm Stürmer, a chemical physicist and radiologist at Siemens Corporation, combined Lehmann’s experience with his own interest in palaeontology and developed new methods of examining the Hünseruck fossils using X-rays [10]. Consequently he produced detailed radiographs of unprepared slates, using soft X-rays (25–40 KV) and stereoscopic exposures, combined with high-resolution films and image processing. These showed some detail of soft tissue not revealed by the conventional techniques that Lehmann had used.

Historical attempts at X-ray imaging of fossil bearing matrix has typically been reported as producing poor results, thought to be due to the density of the material, inclusions in the matrix and lack of resolution of images produced by the equipment used [4]. A major limitation of conventional X-rays was a 2 dimensional image of 3 dimensional structures, resulting in superimposition of all structures in the path of the X-ray beam [4]. Conventional X-rays did not have good differential tissue resolution and thus lacked the ability to provide detailed information about internal structures. Additionally, in the case of fossils, mineralized tissues have similar abilities to absorb X-rays and thus X-ray images were not able to detect difference between these preserved tissues and between them and the surrounding matrix.

Computed Tomography (CT) was invented in 1972 by Godfrey Hounsfield [11]. Compared to conventional X-rays, CT provides higher resolution and cross sectional as well as 3D images. CT additionally has a number of advantages over traditional X-rays. Its greatest benefit perhaps is that it can distinguish between substances of differing densities better than conventional radiographs.

CT was introduced 43 years ago, but its use for palaeoanthropological applications has still to be fully exploited. In 1991, Grine stated that “*the employment of CT in palaeontology is*

potentially even more problematic because diagenetic factors that may affect the mineralization of fossil teeth can only but add to the factors that can confound the use of CT” [12].

It however has been recognized that CT was able to acquire interior information non-destructively from irreplaceable fossil specimens [13,14]. In 1984 Conroy applied CT scanning to a mammalian cranium and after that success he used CT to scan hominin fossils [15]. More detailed studies would follow, with Conroy and others using CT in the analysis of fossil hominin skulls and fossil dental enamel thickness amongst others [12,16,17]. Morphometric studies focusing on such structures as mandibular cross sections [18,19]; femora [20] and labyrinthine structures [21–23] obtained from CT scans were well received, while those on enamel thickness [12] were questioned [24,25].

In palaeoanthropological applications, CT has been used mostly to assess skulls [16,26–30]. But other bones have been examined by CT, including temporal bones, mandibles, femurs and other post cranial elements [18,31–37]. As CT imaging has improved due to software improvements and engineering improvements to equipment, high resolution, modern CT has also been found to be very useful for studying the delicate internal structure of smaller anatomical structures such as the para nasal sinuses, the inner ear and the microanatomy of teeth [21,38–42].

Rapid advances in CT in the 21st century, that run parallel with significant advances in computing technology, as well as software improvements, have made high resolution fossil imaging and reconstruction viable due to expanded CT number scales and the use of special image reformatting software that has provided qualitative and quantitative 3D imaging [6]. Additionally, helical CT—introduced in 1989 [27]—is now significantly better than conventional CT, with higher energy (mAs) capabilities [43]. Thus the combination of software and hardware advances has offered considerably greater potential for the application of CT in palaeontology.

These advances in technology have made the use of CT in the analysis of prepared fossils common place [44]. Most of the CT work to date has been performed on prepared or partially prepared specimens. However, the application of CT to matrix that potentially contains fossils has lagged behind these many advances in the visualization and study of prepared fossils. Very little work has been done to image, via CT, large fossil-bearing matrix conglomerates fresh out of the field. This has, in part, been due to the demand to apply these new technologies to fossils that have already been prepared, or are currently under study, and also to the fact that many matrices that potentially contain fossils have not been previously considered suitable for such imaging, based upon earlier non-rigorous and occasional tests. Furthermore, as palaeontologists and palaeontological technicians have not typically been trained in the interpretation of CT images, the perception seems to have existed that it would be difficult or near impossible to identify fossils still encased in anything but minute amounts of rock. Specifically, previous attempts to use CT to image rocks with potential palaeoanthropological interest has resulted in generally poor results and little effort has been made to apply these methods in the 21st century [4].

Advances in CT technologies, combined with the discovery of sites and localities with denser matrix, containing fewer inclusions have, however, shown promising results for the application of CT technologies to unprepared sediments [45]. A study by Bollinger and colleagues [46] describes the use of multi detector CT in locating, identifying and examining fossil remains of 3 crocodylians embedded in hard shale whilst Rahman and colleagues [47] saw the combination of computer science and the study of past life as creating “an incredibly exciting field”.

In February 2009, a breccia block discovered at Malapa, was found to contain the diaphysis of a humerus (later to be assigned to *A. sediba* MH1). In April 2009, this block was undergoing manual preparation when a portion of a maxilla was uncovered. This maxilla appeared to

belong to an early hominid. Due to its potential importance and prior to further preparation, better visualization was sought of what might be hidden from the preparator's view. On 21 April 2009, the first CT scans of the Malapa material were performed. The visualized maxillary bone was in fact part of an entire juvenile cranium (MH1). The quality of visualization obtained from the CT images gave the first hint that the Malapa calcified clastic sediments were particularly suitable to X-ray penetration.

This discovery also laid the groundwork for the present research and a process of scanning of unprepared blocks was begun.

The aim of this research was to determine the viability of medical CT scanning for use in the identification and characterization of fossils within unprepared matrix blocks from the fossil hominin bearing site of Malapa in the Cradle of Humankind World Heritage site, against the gold standard of traditional block preparation using manual techniques to expose fossils. If successful, such methods could prove cost effective and preserve and protect material, while allowing greater success in discovering and recognizing important fossils.

Materials

The site of Malapa lies to the north of Johannesburg, South Africa in an area known as the Cradle of Humankind (COH)—a UNESCO World Heritage Site declared due to its important hominin fossil-bearing localities [2]. In the late 19th and early 20th century, lime miners traversed this area in search of mineable lime. The lime miners test blasted many sites in their search for economically mineable lime, leaving behind many localities that are only slightly damaged by such activities. The site known as “Malapa” is one such area. It represents a de-roofed cave that has been exposed by years of erosion [3]. After some initial limited blasting, the miners appear to have abandoned further mining activity. Even this limited mining activity, however, left large rocks strewn across the surface of the site. It is some of these rocks that have been collected from the site and taken to what was then the Institute of Human Evolution (IHE) and is now the Evolutionary Studies Institute (ESI) at the University of the Witwatersrand for analysis and examination in this study. The blocks are variable in size. For many of the blocks, their exact context within the fossil deposit on the site is known and recorded, for others, the exact location of recovery is not known, only their presence within the miners' dumps at the site are known as well as their association with the site. The blocks for scanning were chosen due to the presence of visible bone on the exterior of the blocks or due to their potential to yield fossils as determined by their position on the site. 109 blocks were scanned and analyzed. Each block was assigned a “B” number as well as a “UW88” site number for identification purposes.

A medical CT scanner at the Charlotte Maxeke Johannesburg Academic Hospital (CMJAH)—Somatom Definition AS 40 from Siemens (Erlangen, Germany)—was used for the scanning of the 109 blocks. For post processing and interrogation of the medical CT scan data, the images were stored on compact disc (CD) and Digital Imaging and Communication in Medicine (DICOM) images were assessed on an Apple MacBook (Mac OS X version 10.5.8) with OsiriX software (version 3.5.1–64 bit). The CT reader is a diagnostic Radiologist, trained in radiological human anatomy and cross sectional imaging.

Methods

Excavations at the site of Malapa governed by an excavation permit as follows:

Issuing Body: South African Heritage Resources Agency (SAHRA)

Permit Holder: Lee R. Berger

Permit ID: 1946

Case ID: 6407

Validity: 15 January 2015–31 January 2018

The fossil blocks are under the custodial care of the Evolutionary Studies Institute (ESI) at the University of the Witwatersrand, Johannesburg, South Africa.

109 blocks from the Malapa site were scanned. Site/specimen numbers (designated by UW 88) and Block numbers (designated by “B” numbers) were assigned to each block. Preliminary visual identification was made on each block, prior to scanning, of any bone visible on the surface. This identification was done by technical staff of the IHE. Radiographers assisted with the production of the CT images.

CT scanning parameters were chosen—[Table 1](#).

During reconstruction of the raw CT data, kernels are used to enhance spatial and contrast resolution. The kernel is a reconstruction parameter affecting image sharpness and noise by applying a specific mathematical algorithm that digitally filters the raw data during reconstruction. The authors experimented with different kernels, visually assessing the image for suitability of fossil identification. It was found that the H70h was overall best for the specimens scanned. This used a high resolution reconstruction kernel producing a sharper image, although greater noise. This kernel was found to improve bone/fossil visualization with edge enhancement and better spatial resolution. Interpretation of the CT images of the 109 blocks was done prior to block preparation and a colour code was assigned to each block to denote the findings—[Table 2](#)

Following completed analysis of all 109 CT scans, representative blocks were prepared manually by preparators in the IHE. Due to the costly, time consuming nature of manual preparation, 44 blocks were chosen for this manual preparation, after communication between the scientists and the radiologist. Blocks were chosen using a combination of the colour coding assessment assigned from the CT analysis as well as the deemed importance of each block. The latter used visualized surface findings in combination with the deemed importance of the location at which the block was found on the site. The actual specimen findings following manual preparation of these 44 blocks were documented and correlation between the CT findings and the actual findings was made ([Table 3](#)).

Results and Discussion

The surface findings, CT findings and manual preparation findings are tabulated in [Table 3](#) for each block by site/specimen number and block number. The colour code assigned to each block following CT analysis is tabulated. 109 blocks were scanned and 44 manually prepared. The findings are recorded in [Table 3](#).

Unlike fresh living bone, fossilized bone from Malapa has a different CT appearance. Fresh bone appears generally white on CT images with very high, positive Hounsfield unit readings (+700 to +3000 HU), reflecting the calcium content ([Fig 1](#)).

Table 1. CT Scanning parameters used for the scanning of fossil breccia.

| | |
|---------------------|--|
| Matrix size | 512 x 512 |
| Field of View (FOV) | Individualized according to size of rock |
| Slice thickness | 1 mm |
| Pitch | 0.45 |
| mAs | 360 |
| kVp | 140 |

doi:10.1371/journal.pone.0145340.t001

Table 2. Colour assignment depicting CT findings.

| Colour assigned to block | CT Findings |
|--------------------------|--|
| Red | Identifiable bone—probable hominin/primate |
| White | Identifiable bone—not hominin/primate |
| Yellow | Non identifiable bone or absence of bone |

doi:10.1371/journal.pone.0145340.t002

The process of fossilization involves the dissolving and replacement of the original minerals in the bone with other minerals, as well as often crystal formation within spaces and other alterations to the material [48]. This process typically results in a mineralized copy of the original object. The fossil has the same shape as the original object, but is chemically more like a rock. Some of the original bio apatite (a major bone constituent) remains, although it is saturated with silica (rock), calcium carbonate (lime) or other minerals [48]. This results in a change in density and thus appearance and Hounsfield unit reading. Fossilized bone examined in this study, typically appears grey—black on CT with Hounsfield units ranging from +300 to +1500 HU (Fig 2).

Features that were used to help differentiate possible hominin bones from other animal bones were gross skeletal anatomy (if fossils were complete enough), and cortical thickness—hominin limb bones typically having thicker cortical bone than other non—hominin bones (the thickness being relative when compared to the whole bone thickness) [49].

On analysis of the correlation of the CT findings and the manual preparation findings the following were found:

31 of the 44 blocks prepared (70.5%) had concordant findings on CT and actual preparation.

9 of the 44 cases (20.4%) showed minor variances.

4 of the 44 cases (9.1%) were discordant.

Results were deemed to be concordant when the CT predictions of the identification of the bone as well as the taxonomic designation were the same as findings on manual preparation—(Figs 3 and 4). Discordant results arose when the prediction of findings from the CT had mis—identified the bones, when correlated with the actual findings post manual preparation. Minor variances were assigned when the CT had predicted the type of bone but was unable to identify the specific bone or the bone was mis-assigned taxonomically. Manual preparation then confirmed the identification of the bone. This occurred when the bone was small and fragmentary, making CT identification difficult.

Examination of the 9 cases of minor variance where CT had predicted the type of bone but could not identify further showed that this was due to several factors:

1. Where the bone was found to be crushed and fragmented, accuracy of prediction diminished with partial voluming causing erroneous appearances on CT—which were interpreted as bony anatomy.
2. CT over predicted possible hominin bones. Hominin prediction was done predominantly by assessing relative cortical thickness, and over estimation could have been due to similar density matrix making accurate cortical thickness measurement difficult.
3. The size of the fossil bones correlated with the accuracy of prediction. Bigger bones were more easily correctly identified from CT images than were small bones.

Table 3. CT findings vs preparation findings.

| UW Number | Block number | Scan venue | Priority | Surface ID | CT Findings | Volume cm ³ | Preparation findings | CT vs preparation findings |
|-----------|--------------|------------|----------|---------------------------|---------------------------------|------------------------|---|----------------------------|
| UW88-1316 | B001 | CMJAH | yellow | nil | nil | 12304 | Unidentified fragment | concordant |
| UW88-1342 | B027 | CMJAH | yellow | nil | fragments | 862 | Pelvic fragment | concordant |
| UW88-1365 | B050 | CMJAH | red | nil | Phalanx, long bone (tibia/ulna) | 1451 | Distal bovid metapodial, bovid metacarpal | minor variance |
| UW88-1368 | B053 | CMJAH | yellow | Bone fragments | fragments | 285 | Bone fragments | concordant |
| UW88-1376 | B061 | CMJAH | white | nil | Long bone (tibia) | 2672 | | |
| UW88-1388 | B073 | CMJAH | white | nil | Femoral head | 60 | Bovid vertebra | discordant |
| UW88-1393 | B078 | CMJAH | yellow | nil | nil | 238 | | |
| UW88-1396 | B081 | CMJAH | yellow | nil | Crystal, crushed bone | 1030 | | |
| UW88-1421 | B106 | CMJAH | yellow | nil | Fragments | 496 | Fragments | concordant |
| UW88-1428 | B113 | CMJAH | yellow | nil | Long bone fragments | 919 | Carnivore metacarpal and long bone. Small mammal humerus and tibia | minor variance |
| UW88-1440 | B125 | CMJAH | red | nil | Fragments, possible scapula | 418 | Fragments. Parts of flat bone and long bone with cortical manganese | minor variance |
| UW88-1443 | B128 | CMJAH | yellow | Bovid antler fragment | Long bone fragment | 41 | | |
| UW88-1456 | B141 | CMJAH | yellow | nil | fragments | 782 | 1 st proximal phalanx, lateral end clavicle | minor variance |
| UW88-1462 | B147 | CMJAH | yellow | nil | nil | 1297 | | |
| UW88-1472 | B157 | CMJAH | yellow | nil | fragments | 1932 | fragments | concordant |
| UW88-1476 | B161 | CMJAH | yellow | Long bone | Surface bone | 897 | | |
| UW88-1479 | B164 | CMJAH | yellow | nil | Long bone | 1700 | Cervical vertebra bovid | discordant |
| UW88-1483 | B168 | CMJAH | yellow | nil | nil | 2843 | Tiny caudal vertebra bovid | discordant |
| UW88-1487 | B172 | CMJAH | yellow | Microfauna (tooth) | nil | 682 | | |
| UW88-1491 | B176 | CMJAH | yellow | nil | nil | 190 | | |
| UW88-1505 | B190 | CMJAH | yellow | fragment | fragment | 2522 | fragment | concordant |
| UW88-1506 | B191 | CMJAH | white | Rib fragment, micro fauna | Ulna bovid | 473 | | |
| UW88-1523 | B208 | CMJAH | red | micro fauna | Malleolus/tibia ball joint | 111 | | |
| UW88-1557 | B242 | CMJAH | yellow | nil | Long bone bovid | 293 | | |

(Continued)

Table 3. (Continued)

| UW Number | Block number | Scan venue | Priority | Surface ID | CT Findings | Volume cm ³ | Preparation findings | CT vs preparation findings |
|-----------|--------------|------------|----------|---|--|------------------------|---|----------------------------|
| UW88-1560 | B245 | CMJAH | red | nil | Hominin vertebra and rib | 5387 | Lumbar vertebra and rib from <i>A. sediba</i> . Body rib bovid II | concordant |
| UW88-1564 | B249 | CMJAH | yellow | Flow stone | Tubular bone | 2720 | | |
| UW88-1566 | B251 | CMJAH | yellow | nil | Long bone fragment | 1113 | | |
| UW88-1578 | B263 | CMJAH | yellow | Bovid rib fragment | Fragments | 3797 | | |
| UW88-1586 | B271 | CMJAH | white | nil | Primate ribs, long bone fragments, artefact ++ | 4802 | | |
| UW88-1594 | B279 | CMJAH | yellow | nil | Fragments | 5364 | | |
| UW88-1600 | B285 | CMJAH | yellow | Long bone fragment | fragments | 3635 | | |
| UW88-1601 | B286 | CMJAH | yellow | nil | Long bone fragments | 195 | calcaneus | discordant |
| UW88-1613 | B298 | CMJAH | yellow | nil | Fragments | 2269 | | |
| UW88-1629 | B314 | CMJAH | yellow | nil | Fragments | 2224 | Fragments | concordant |
| UW88-1631 | B315b | CMJAH | yellow | nil | Fragments | 7984 | | |
| UW88-1638 | B322 | CMJAH | yellow | Small mammal | nil | 5491 | | |
| UW88-1650 | B334 | CMJAH | yellow | Snails, fly pupae, manganese, flowstone | fragments | 7182 | | |
| UW88-1654 | B338 | CMJAH | white | nil | 2 long bones (tibia/fibula) | 792 | Juvenile bovid tibia + fibula shaft fragments | concordant |
| UW88-1656 | B340 | CMJAH | white | fragments | Ribs/long bones | 2987 | Ribs + long bones | concordant |
| UW88-1658 | B342 | CMJAH | yellow | nil | Fragments | 1362 | | |
| UW88-1670 | B354 | CMJAH | white | nil | Fragments, mandible piece | 1782 | Bovid III mandible ramus + fragments | concordant |
| UW88-1687 | B371 | CMJAH | white | nil | Long bone | 1833 | | |
| UW88-1691 | B375 | CMJAH | white | nil | Ribs articulating with vertebrae, long bone, artefact ++ | 4315 | 5 x Articulated sub adult bovid vertebrae, with 2 ribs. Possible primate ulna | concordant |
| UW88-1695 | B379 | CMJAH | white | Pupae | Complex bone shape, rib | 4316 | Canid mandible, ribs | minor variance |
| UW88-1704 | B388 | CMJAH | yellow | nil | Thin curved bone, cranial fragments, artefact ++ | 2356 | Bovid phalanx and skull fragments | concordant |
| UW88-1705 | B389 | CMJAH | yellow | Rat mandible | Fragments | 1237 | | |
| UW88-1718 | B402 | CMJAH | yellow | Fragments | nil | 8733 | | |
| UW88-1728 | B412 | CMJAH | yellow | Fly pupae, rock fragments | Bone fragments | 1274 | | |

(Continued)

Table 3. (Continued)

| UW Number | Block number | Scan venue | Priority | Surface ID | CT Findings | Volume cm ³ | Preparation findings | CT vs preparation findings |
|-----------|--------------|------------|----------|--|--|------------------------|--|----------------------------|
| UW88-1729 | B413 | CMJAH | yellow | nil | nil | 10087 | nil | concordant |
| UW88-1733 | B417 | CMJAH | yellow | ? Bird bone, insect damage | nil | 3349 | | |
| UW88-1753 | B437 | CMJAH | yellow | ? Rabbit tooth | Fragments | 477 | | |
| UW88-1754 | B438 | CMJAH | yellow | Dolomite inclusion | Fragments bone | 1092 | | |
| UW88-1758 | B442 | CMJAH | white | nil | Vertebral elements, ribs | 3403 | Bovid vertebrae and ribs | concordant |
| UW88-1762 | B446 | CMJAH | white | nil | Long bone -crushed | 1286 | | |
| UW88-1769 | B453 | CMJAH | red | nil | Fragments | 420 | Crushed bone fragments | concordant |
| UW88-1781 | B465 | CMJAH | white | nil | Bovid vertebra | 3656 | Thoracic bovid III vertebra | concordant |
| UW88-1785 | B469 | CMJAH | white | Clay nodules | Flat bone, fragments | 1395 | Flat bone fragment | concordant |
| UW88-1789 | B473 | CMJAH | yellow | Fragments, micro fauna, ? burrows | Fragments bone | 3063 | | |
| UW88-1791 | B475 | CMJAH | yellow | Fly pupae | Fragments bone | 2615 | | |
| UW88-1792 | B476 | CMJAH | yellow | ? Burrows | Small cube-like objects | 2537 | | |
| UW88-1793 | B477 | CMJAH | yellow | nil | nil | 1370 | | |
| UW88-1799 | B483 | CMJAH | yellow | Fragments bone, quartz | Fragments bone | 3547 | | |
| UW88-1806 | B490 | CMJAH | white | nil | Bone fragments, distal femur, ribs/flat bone | 2778 | Bovid II distal femur, rib fragments bovid III | concordant |
| UW88-1807 | B491 | CMJAH | white | Bovid mandible | Mandible with teeth | 9625 | Bovid mandible and teeth | concordant |
| UW88-1812 | B496 | CMJAH | yellow | nil | Fragments bone | 1587 | Bone fragments | concordant |
| UW88-1813 | B497 | CMJAH | yellow | Long bone shaft fragment | Unidentifiable bone | 5739 | | |
| UW88-1816 | B500 | CMJAH | yellow | nil | Bone fragments | 3419 | Bone fragments | concordant |
| UW88-1822 | B506 | CMJAH | yellow | CaCO ₃ stalactite, snail shells | Fragments bone | 1804 | Fragment mammalian rib | minor variance |
| UW88-1833 | B517 | CMJAH | white | nil | Vertebral, rib and long bone fragments | 4378 | | |
| UW88-1834 | B518 | CMJAH | yellow | Fragments | Fragments bone | 3806 | | |
| UW88-1836 | B520 | CMJAH | yellow | nil | Fragments bone | 5699 | | |
| UW88-1840 | B524 | CMJAH | yellow | ? stone tools | nil | 4384 | | |
| UW88-1845 | B529 | CMJAH | yellow | inclusion | Fragments bone | 2155 | | |

(Continued)

Table 3. (Continued)

| UW Number | Block number | Scan venue | Priority | Surface ID | CT Findings | Volume cm ³ | Preparation findings | CT vs preparation findings |
|-----------|--------------|------------|----------|------------------------------------|--------------------------------|------------------------|--|----------------------------|
| UW88-1853 | B537 | CMJAH | yellow | Rock inclusion, fly pupae | Fragments | 1013 | | |
| UW88-1857 | B541 | CMJAH | yellow | Dolomite inclusion | Fragments bone | 2786 | | |
| UW88-1860 | B544 | CMJAH | yellow | nil | Fragments bone | 3564 | | |
| UW88-1862 | B546 | CMJAH | yellow | nil | Fragments bone | 1891 | Bone fragments | concordant |
| UW88-1863 | B547 | CMJAH | yellow | Rock flakes | Fragments bone | 2180 | | |
| UW88-1870 | B554 | CMJAH | white | nil | Long bones, vertebra, rib | 1712 | Small cat pelvis in articulation with vertebra and femur | minor variance |
| UW88-1871 | B555 | CMJAH | yellow | Clay nodule | Fragments bone | 1234 | | |
| UW88-1876 | B560 | CMJAH | red | nil | Long bone fragment | 5817 | Long bone fragments | concordant |
| UW88-1877 | B561 | CMJAH | yellow | nil | nil | 2422 | | |
| UW88-1879 | B563 | CMJAH | yellow | Dolomitic inclusion, rib fragment | Fragments bone, artefact ++ | 2535 | | |
| UW88-1887 | B571 | CMJAH | yellow | nil | nil | 1390 | | |
| UW88-1888 | B572 | CMJAH | yellow | Fly pupae | nil | 1853 | | |
| UW88-1904 | B588 | CMJAH | white | nil | Rib fragment, metapodial | 1164 | | |
| UW88-1905 | B589 | CMJAH | white | nil | Flat bone | 1717 | Flat bone | concordant |
| UW88-1906 | B590 | CMJAH | yellow | Rock flake, fly pupae, snail shell | Fragments | 1005 | Bovid 2 nd phalanx fragment | minor variance |
| UW88-1910 | B594 | CMJAH | white | Air pockets | Long bone fragment | 1727 | | |
| UW88-1912 | B596 | CMJAH | yellow | nil | Long bone fragment, artefact++ | 4985 | Bird tibia—proximal fragment | minor variance |
| UW88-1918 | B602 | CMJAH | yellow | ? Burrows | Bone fragment | 2444 | | |
| UW88-1925 | B609 | CMJAH | yellow | airspace | Fragments | 1305 | | |
| UW88-1932 | B616 | CMJAH | yellow | nil | Bone fragments | 1064 | | |
| UW88-1943 | B627 | CMJAH | yellow | nil | nil | 1310 | | |
| UW88-1951 | B635 | CMJAH | yellow | nil | Fragments | 1010 | | |
| UW88-1954 | B638 | CMJAH | yellow | Fragments bone | Fragments bone | 939 | | |
| UW88-1955 | B639 | CMJAH | red | ? Burrows, ? organics | Distal femur/proximal tibia | 1365 | Proximal tibia | concordant |
| UW88-1962 | B646 | CMJAH | yellow | nil | nil | 1113 | | |

(Continued)

Table 3. (Continued)

| UW Number | Block number | Scan venue | Priority | Surface ID | CT Findings | Volume cm ³ | Preparation findings | CT vs preparation findings |
|-----------|--------------|------------|----------|----------------------|---------------------|------------------------|----------------------|----------------------------|
| UW88-1971 | B655 | CMJAH | yellow | nil | Bone fragments | 457 | Bone fragments | concordant |
| UW88-1972 | B656 | CMJAH | yellow | Microfauna, dolomite | Fragments | 924 | | |
| UW88-1988 | B672 | CMJAH | yellow | Fly pupae | Bone fragments | 2613 | | |
| UW88-1999 | B683 | CMJAH | white | Burrows | Pelvic fragment | 827 | Pelvic fragment | concordant |
| UW88-2008 | B692 | CMJAH | white | nil | Femur large bovid | 944 | Distal bovid femur | concordant |
| UW88-2014 | B698 | CMJAH | white | nil | Bone fragment | 2094 | Bovid bone fragments | concordant |
| UW88-2040 | B724 | CMJAH | yellow | Dolomite/quartz | Long bone fragments | 2481 | | |
| UW88-2044 | B728 | CMJAH | yellow | nil | fragments | 1329 | | |
| UW88-2015 | B735 | CMJAH | yellow | nil | Fragments | 2258 | | |
| UW88-2053 | B737 | CMJAH | yellow | nil | Fragments | 738 | Fragments | concordant |
| UW88-2386 | B1070 | CMJAH | yellow | nil | nil | 680 | | |

doi:10.1371/journal.pone.0145340.t003

Analysis of the 4 cases where there was CT/preparation discordance showed:

1. Size of specimen again played a role in accuracy of assessment. Smaller bones were more easily missed or mis-identified.
2. Artifact contributed to poor CT- preparation correlation.
3. Complex bony architecture, such as facial bones and pelvises, were more difficult that tubular, long bones, to correctly identify.
4. Vertebrae were somewhat problematic, especially when small.
5. In 2 cases, (B164 and B286), the discordance was thought to be due to confusion in block numbering with the blocks scanned not in fact being the blocks prepared.

The CT images of the discordant cases were re-evaluated following preparation findings. Re-evaluation could not convincingly find the bones that had originally been missed, nor improve identification of visualized bones. As round shapes may be poorly seen in a single plane, careful multi planar evaluation was done, but this did not improve their identification. Visualization of each scan in multiple planes was shown to be essential for complete evaluation, as objects could sometimes be well seen in one projection, but poorly visualized in an orthogonal view [50]—tubular structure (long bones *etc.*) are well seen when viewed along their long axis but less well seen if only a transverse, short axis is viewed. These findings might suggest that the round shape is more easily missed on CT viewing, as several of the dissimilar cases, involved vertebrae or a calcaneus—the common factor here seemingly possibly the shape, although cataloguing error (where block numbers was changed between CT scanning and manual preparation) was strongly suspected in a couple of the cases.

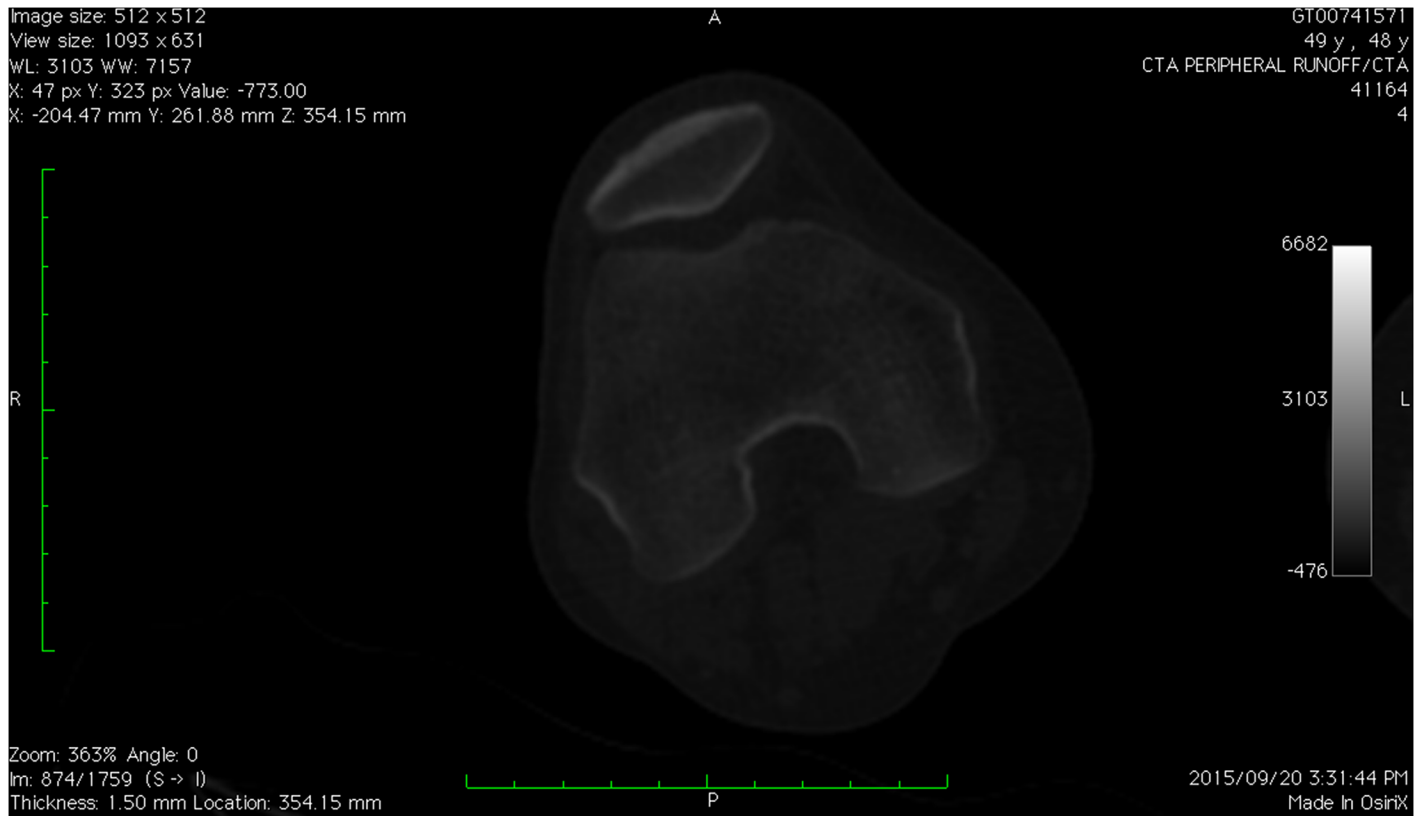


Fig 1. CT image of a distal femur of a living human—fresh bone. The cortex of the bone appears white with the mineralized matrix also appearing as shades of white to grey. Basic iterative reconstruction technique. Scale = 10 cm total—each bar = 1 cm.

doi:10.1371/journal.pone.0145340.g001

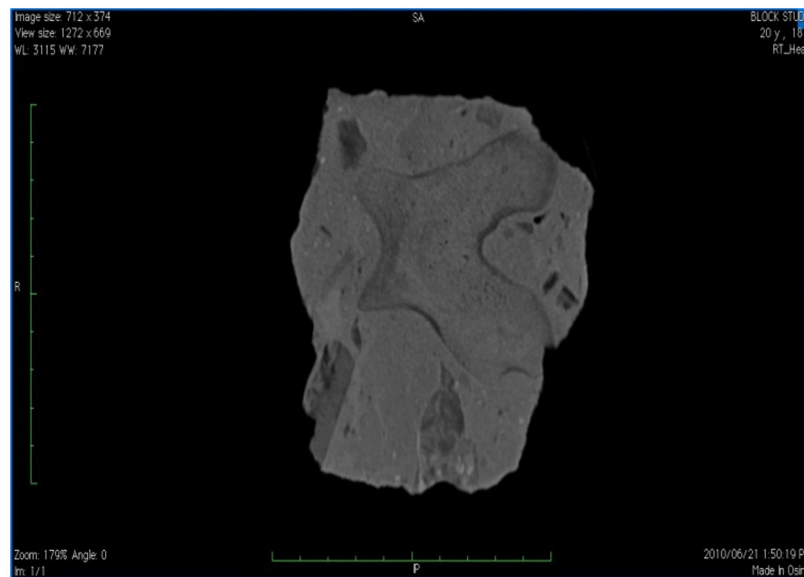


Fig 2. CT image of fossil of a distal bovid femur embedded entirely in matrix. The edges of the fossil appear dark grey. The central body of the fossil is of a very similar grey colour to the surrounding matrix. Small air pockets and inclusions appear black or nearly black. H70h kernel used. Scale = 10 cm total—each bar = 1 cm.

doi:10.1371/journal.pone.0145340.g002

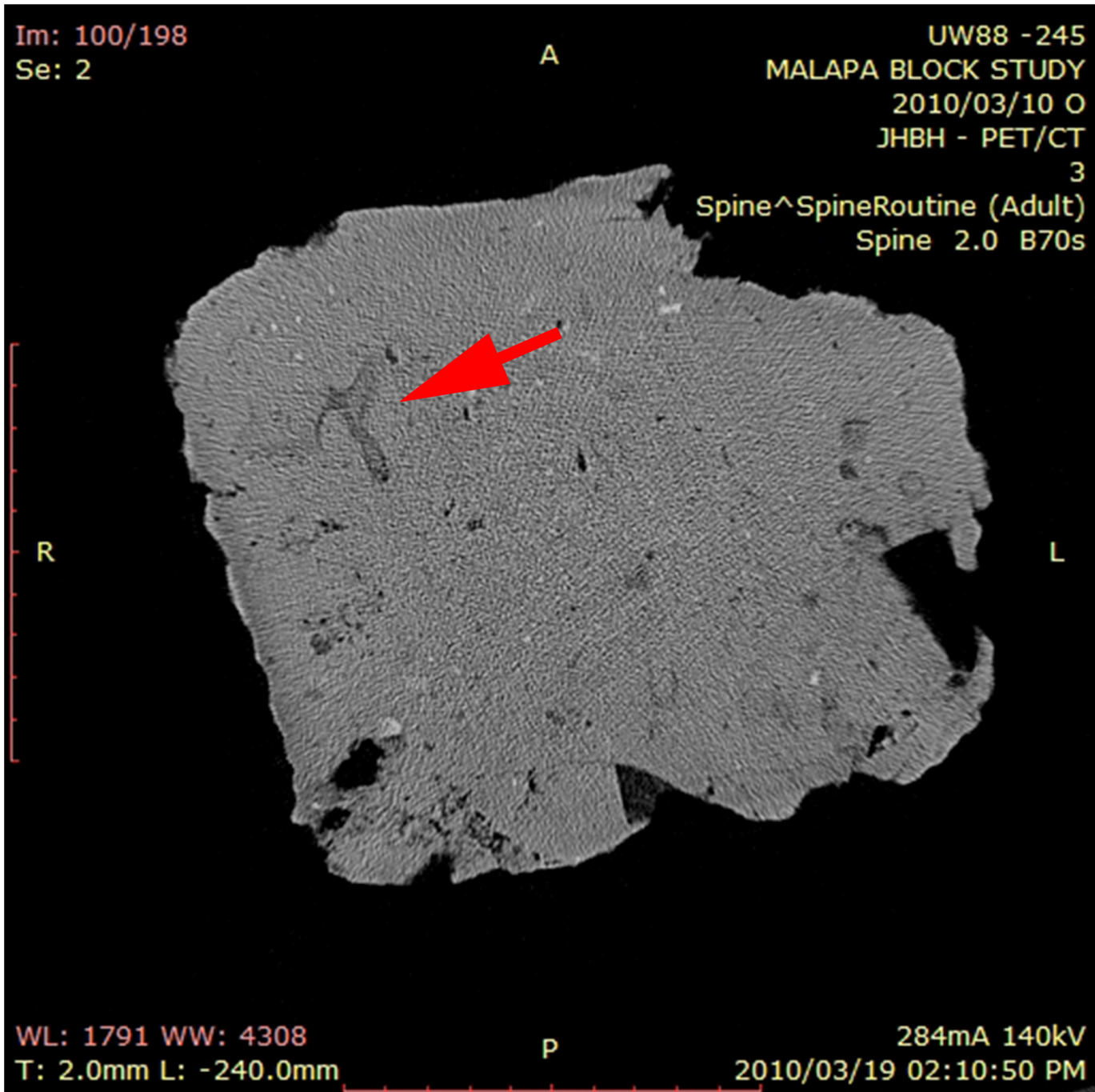


Fig 3. B 245 (UW 88–152)—Hominin vertebra identified on CT (arrow). Seen in sagittal projection.

doi:10.1371/journal.pone.0145340.g003

Importantly it was noted that when viewing, the CT image should be magnified according to the object being sought. As the FOV varies according to block size, all images are initially processed to occupy the same viewer space, regardless of the blocks' true size. Thus small objects may be very difficult to find unless the image is magnified so that the visualized size of an object mimics more closely its true size. Magnification during viewing causes enlargement of a small area by selecting that small area within the total digital field and making it cover the



Fig 4. B 245 (UW88 152)—*Australopithecus sediba*'s vertebra after preparation.

doi:10.1371/journal.pone.0145340.g004

full display. This differs from the process of changing the FOV during image reconstruction. Reducing the FOV has the effect of increasing image detail, magnification does not do this. Without adjustment of the magnification when viewing, perspective is forgotten and smaller fossils e.g. teeth may be overlooked.

Medical CT has, over time, become standardized due to the fact that there are a limited number of different scanning subjects [50]. However, in contrast, the use of CT for palaeontological investigations requires case by case selection of scanning parameters to optimize the contrast between objects of interest whilst minimizing artifact.

Grey scale is the way in which the grey shades in a black and white image are spread. The grey shades are correlated with the digital pixel values of the image, with ranges of pixel values assigned to a certain grey shade. The CT machine will allow one to determine which matrix number should be printed as white and which should be printed as black. The numerical range between the white and black levels establishes the CT window "width". "Window width" is defined as the range of CT numbers (in Hounsfield units) included in the grey—scale display of the CT image, ranging from 1 to 2000 or 3000, depending on the type of machine. The centre of that numerical range becomes the window "level". The window width is divided by sixteen to determine the numbers which are included in each individual grey tone.

A grey scale on the display will typically contain 256 grey shades [51], whereas the Hounsfield scale has 4096 values. The range of grey scale units used during post processing varies from the Hounsfield unit scale generated by the CT machines as most medical CT systems use a 12-bit scale where 4096 values are possible, but the post processing software makes use of 16 or 64-bit scales where the range is 0–65 535 [50]. This scale does not purport to equate to the actual density of the geological materials, but allows relative comparison of densities. Ketcham et al [50] when commenting on CT use for geosciences states that "For geological purposes, it is commonly more desirable to select the reconstruction parameters to maximize the CT-value contrast for each scanned object. This makes viewer experience with image processing essential for accurate interpretation."

The human observer can perceive no more than around 900 shades of gray. Therefore, there is an upper limit to the amount of grayscales in a medical viewing application. Display systems that are able to show 1,024 simultaneous shades of gray (10 bits) are sufficient for medical imaging. Display systems exceeding this specification will present to the human observer shades of gray that cannot be discriminated from each other anymore. [52]

The grey scale of the individual images was adjusted to reach a “best view” depiction of block contents. It has been noted by CT researchers that it is possible to set the window inappropriately and completely miss the important diagnostic information from a particular study [53]. If the window is set too wide, each grey tone will include such a wide range of tissue density that a potential object is likely to be indistinguishable from the surrounding material.

The CT reader is trained in anatomical bony recognition and has training and significant experience in digital imaging. As noted by several authors [50,54], this is essential for accurate CT prediction of fossil findings. Readers need to be familiar with the complexities of CT post processing and image manipulation as findings can be “lost” in the CT image, should the incorrect manipulations be performed or poor settings used for viewing. [54,55]

Artifact production can degrade the CT image and hinder interpretation. Modern CT machines are developed with built-in artifact reduction features, including filters, calibration correction, automatic tube current modulation and scanner software [56]. Artifact noted on the CT scans in this study was more marked in the breccia of larger volume, but interpretation was still possible. Beam hardening artifact was identified to varying degrees on the CT scans as streaking emanating from the rock’s surface and through the rock. Willis *et al* [57] showed that the higher photon attenuation and irregular shape of fossilized material lead to severe streak artifact resulting from abrupt changes in X-ray transmission intensity across an object and was often associated with long straight edges of high attenuation material. Scanning at a higher kV results in a harder X-ray beam, and thus less beam hardening artifacts, hence the choice of the maximum KVp of 140 on the medical scanner.

Of note, was that no hominin fossils were missed on CT predictions, in blocks prepared. This may be due to the general relative thicker cortices [49] of hominin bones over other animals, thus facilitating their identification even when round in shape. Not only was CT convincingly able to identify the presence of fossil bone, but good visualization allowed good predictive identification and characterization. CT scans offer a quick and non-destructive method of imaging. Data is obtained in a digital format that allows 3 dimensional representations of an object to be created. Post processing of this data allows reconstructions, measurements and a variety of analyses to be performed.

There are however limitations to the use of CT in palaeontological research, many of these are being overcome as hardware and software improvements occur and advancements in technology are made. The CT image can be manipulated and visualized depending on the required application. Often 2 D analyses along orthogonal planes are sufficient for skeletal structures, but additional information can be gained from 3 D image reconstructions. Traditionally these 3D reconstructions are calculated from CT values based on CT grey scale numbers. If quantitative measurements are needed from the CT data, segmentation techniques are often necessary to separate features of interest based on criteria other than CT values, as use of CT numbers may be complicated by partial volume averaging effects [58]. Manipulation of CT parameters at the time of scanning, to lessen imaging artifact, can hinder precise image acquisition [59]. Partial voluming and limits in spatial resolution are important constraints of CT [23]. Scientists have tested and validated the accuracy of these latter two constraints as regards the accuracy and reproducibility of measurements and the definition of landmark coordinates [60–62].

The use of medical CT was specifically investigated, as oppose to industrial CT with micro CT capabilities or other scanning technologies (e.g. synchrotron) for the following reasons:

- Industrial micro CT is presently not readily available in South Africa [55], scanning times are longer than medical CT (hours versus seconds on a medical scanner) [63] and size and weight restrictions on these micro CT machines are significantly more limiting than on medical CT scanners. (The micro CT at the University of Witwatersrand takes a maximum diameter of +/- 20 cm and a weight of 50–60 kg, whereas medical CT allows diameter of 80–90 cm and weights of between 200–300 kg).
- Synchrotron scanners are very scarce, immensely costly and very time consuming.
- Both micro CT and synchrotron imaging generate very large data sets, necessitating dedicated computers and software with large data handling capabilities. These are expensive and not as freely available as ordinary laptop or desktop computers that can handle the DICOM data generated from the medical scanner. In addition, medical CT data can be analyzed with software that is free.

Conclusions

In 2009, Wu [4] stated “*The suitability of medical CT for the study of hominin fossils is limited by its low X-ray dosage that is unable to penetrate highly mineralized and matrix-filled specimens.*” Scanning of 109 matrix fossil-bearing rocks from the site of Malapa yielded CT images of a quality that, coupled with modern software post processing programmes and a suitably trained and experienced reader, allowed for the accurate prediction of the fossil contents of the blocks.

Medical CT scanners are shown by this study to be capable of producing images that allow for the accurate identification and often characterization of fossils. The correlation of these predicted findings with the actual findings post manual preparation is sufficiently concordant to change the traditional course of the handling of fossil bearing blocks. In order to maximize the use of limited resources and manual preparatory skills as well as to curtail costs, this research suggests that prior to manual preparation, blocks should undergo scanning with medical CT scanners and “virtual” assessment of contents should be undertaken by suitably qualified individuals to allow for prioritization of rocks for manual preparation. Knowledge of bony as well as radiological anatomy is deemed essential for accurate interpretation of findings, as is familiarity and experience with digital imaging techniques, their production limitations and pit falls of post processing manipulation.

For the first time in South African palaeoanthropological work hominin fossils have been imaged within their matrix before any preparation had been performed. The relationships of all the bones could be eloquently demonstrated on post-processing of the CT images. This afforded scientists the unique opportunity to, up front, assess and plan the further investigation and preparation of this block—something never achieved in South Africa before.

The results of this study have shown conclusively the viability and value of the use of medical CT imaging to assess possible fossil-containing rocks for fossil remains. It has also demonstrated that there is considerable advantage to being able to know the contents of a rock ahead of costly, time-consuming “blind” manual preparation. This allows decisions to be made as regards the most efficient use of resources, manpower and allocation of funds, in addition to allowing planning of the course of action for each fossil. Information can be extracted without damage to the matrix and hence allows the potential for preservation of these remains for future generations of scientists, ensuring that as technology advances, enough direct physical evidence has been left behind on which to apply new methods of analysis in the future.

Acknowledgments

Evolutionary Studies Institute (ESI), University of the Witwatersrand and National Palaeosciences Centre of Excellence

Carlson K; De Klerk B; Kibii, J; Languza R; Lawrence W; Mukanku J; Nyalunga M; Randolph-Quinney P; Thackeray F; Val A

Department of Nuclear Medicine, Charlotte Maxeke Johannesburg Academic Hospital (CMJAH)

Maleeme D; Padiachy S; Vangu MDT

Department of Diagnostic Radiology, Charlotte Maxeke Johannesburg Academic Hospital

Letsoalo Q

Charlotte Maxeke Johannesburg Academic Hospital

Author Contributions

Conceived and designed the experiments: LRB JSS. Performed the experiments: JSS. Analyzed the data: JSS. Contributed reagents/materials/analysis tools: JSS LRB. Wrote the paper: JSS LRB.

References

1. Berger L. R. (2005) Working and Guiding in the Cradle of Humankind. Prime Origins Publishing.
2. UNESCO (2012) World Heritage List.
3. Dirks PHGM, Kibii JM, Kuhn BF, Steininger C, Churchill SE, Kramers JD, et al (2010) Geological setting and age of Australopithecus sediba from southern Africa. *Science* 328: 205. doi: [10.1126/science.1184950](https://doi.org/10.1126/science.1184950) PMID: [20378812](https://pubmed.ncbi.nlm.nih.gov/20378812/)
4. Wu X, Schepartz LA (2009) Application of computed tomography in palaeoanthropological research. *Progress in Natural Science* 19: 913–921.
5. du Plessis A, Steyn J, Roberts DE, Botha LR, Berger LR (2013) A proof of concept demonstration of the automated laser removal of rock from a fossil using 3D X- ray tomography data. *Journal of Archaeological Science* 40: 4607–4611.
6. Cunningham JA, Rahman IA, Lautenschlager S, Rayfield EJ, Donoghue PJC (2014) A virtual world of paleontology. *Trends in Ecology and Evolution* 29: 347–357. doi: [10.1016/j.tree.2014.04.004](https://doi.org/10.1016/j.tree.2014.04.004) PMID: [24821516](https://pubmed.ncbi.nlm.nih.gov/24821516/)
7. Brühl (1896) Ueber die verwendung von Rontgenschen X-Strahlen zu palaeontologischdiagnostischen Zwecken.—verhandlungen d. Berliner Physiologischen. *Arch Anat Physiol, Physiologische Teil* 547–550.
8. Lemoine M (1896) De l'application des rayons de Rontgen a la paleontologie. *C R Acad Sci* 123: 764–765.
9. Hohenstein P (2004) X-ray imaging for palaeontology. *BJR* 77: 420–425. PMID: [15121706](https://pubmed.ncbi.nlm.nih.gov/15121706/)
10. Selden P. and Nudds J. (8-31-2011) Evolution of Fossil Ecosystems. Manson Publishing.
11. Hounsfield GN (1973) Computerized transverse axial scanning (tomography). Part 1: description of system. *British Journal of Radiology* 46: 1016–1022. PMID: [4757352](https://pubmed.ncbi.nlm.nih.gov/4757352/)
12. Grine FE (1991) Computed tomography and the measurement of enamel thickness in extant hominoids: implications for its palaeontological application. *Palaeont Afr* 28: 61–69.
13. Conroy GC, Vannier MW (1984) Non-invasive three dimensional computer imaging of matrix-filled skulls by high resolution computed tomography. *Science* 226: 456–458. PMID: [17799939](https://pubmed.ncbi.nlm.nih.gov/17799939/)

14. Haubitz B, Prokop M, Dohring W, Ostron JH, Wellnhofer P (1988) Computed tomography of Archaeopteryx. *Paleobiology* 14: 206–213.
15. Vannier MW, Conroy GC, Marsh JL, Knapp RH (1985) Three-dimensional cranial surface reconstructions using high resolution computed tomography. *Journal of Physical Anthropology* 67: 299–311.
16. Conroy GC, Vannier MW, Tobias PV (1990) Endocranial features of *Australopithecus africanus* revealed by 2- and 3-D computed tomography. *Science* 247: 838–841. PMID: [2305255](#)
17. Schwatz GT, Thackeray JF, Reid C, V Reenan JF (1998) Enamel thickness and the topography of the enamel-dentine junction in South African Plio-Pleistocene hominids with special reference to Carabelli trait. *Journal of Human Evolution* 35: 523–542. PMID: [9774509](#)
18. Daegling DJ, Grine FE (1991) Compact bone distribution and biomechanics of early hominid mandibles. *American Journal of Physical Anthropology* 86: 321–339. PMID: [1746641](#)
19. Schwatz GT, Conroy GC (1996) Cross sectional geometric properties of the Otavipithecus mandible. *American Journal of Physical Anthropology* 99: 613–623. PMID: [8779342](#)
20. Ohman JC, Krochta TJ, Lovejoy CO, Mensforth RP, Latimer B (1997) Compact bone distribution in the femoral neck of hominoids: implications for the locomotion of *Australopithecus aferensis*. *American Journal of Physical Anthropology* 104: 117–131. PMID: [9331457](#)
21. Spoor F, Wood B, Zonneveld F (1994) Implication of early hominid labyrinthine morphology for the evolution of human bipedal locomotion. *Nature* 369: 645–648. PMID: [8208290](#)
22. Spoor, C. F. (1993) The comparative morphology and phylogeny of the human bony labyrinth [dissertation]. University of Utrecht.
23. Spoor CF, Zonneveld F (1995) Morphometry of the primate bony labyrinth: a new method based on high resolution computed tomography. *J Anat* 186: 271–286. PMID: [7649826](#)
24. Spoor CF, Zonneveld F, Macho GA (1993) Linear measurement of cortical bone and dental enamel by computed tomography: applications and problems. *Journal of Physical Anthropology* 91: 469–484.
25. Conroy GC (1991) Enamel thickness in South African australopithecines: Non invasive evaluation by computed tomography. *Palaeont Afr* 28: 53–59.
26. Wu XJ, Liu W, Dong W, Que JM, Wang YF (2008) The brain morphology of Homo Liujiang cranium fossil by three dimensional computed tomography. *Chinese Science Bulletin* 53: 2513–2519.
27. Falk D, Hildebolt C, Smith K, Morwood MJ, Sutikna T, Brown P, et al (2005) The brain of LB1 *Homo floresiensis*. *Science* 308: 242–245. PMID: [15749690](#)
28. Balzeau A, Grimaud-Hervé D, Jacob T (2005) Internal cranial features of the Mojokerto child fossil (East Java, Indonesia). *J Hum Evol* 48: 535–553. PMID: [15927659](#)
29. Falk D, Clarke R (2007) Brief communication: new reconstruction of the Taung endocast. *American Journal of Physical Anthropology* 134: 529–534. PMID: [17786995](#)
30. Conroy GC, Weber GW, Seidler H, Tobias PV, Kane A, Brunson B (1998) Endocranial capacity in an early hominid cranium from Sterkfontein, South Africa. *Science* 280: 1730–1731. PMID: [9624045](#)
31. Fairdough I (2010) CT scans offer a new way of looking at fossils.
32. Junger WL, Minns RJ (1979) Computed tomography and biochemical analysis of fossil long bones. *American Journal of Physical Anthropology* 50: 285–290. PMID: [109011](#)
33. Daniels R (2011) Technologies Used in Investigating Fossils.
34. Stewart K (2009) Famous fossil Lucy scanned at the University of Texas at Austin, offers new insights into Ancient Human Ancestor.
35. McLean D, Robinson J, Archer M (2001) Artefact reduction on CT images of fossils to allow 3D visualisation. *Radiation Physics and Chemistry* 61: 723–724.
36. Ruff CB (1994) Morphological adaptation to climate in modern and fossil hominids. *American Journal of Physical Anthropology* 37: 65–107.
37. Galik K, Senut B, Pickford M, Gommery D, Treil J, Kuperavage AJ, et al. (2004) External and Internal morphology of the BAR 1002' 00 *Orrorin tugenensis* femur. *Science* 305: 1450–1453. PMID: [15353798](#)
38. Manzi G, Bruner E, Caprasecca S, Gualdi G, Passarello P (2001) CT scanning and virtual reproduction of the Saccopastore Neanderthal crania. *Riv Antro* 79: 61–72.
39. Prossinger H, Seidler H, Wicke L, Weaver D, Recheis W, Stringer C, et al (2003) Electronic removal of encrustations inside the Steinheim cranium reveals para nasal sinus features and deformations and provides a revised endocranial volume estimate. *Anat Rec B* 273: 132–144.
40. Plotino G, Grande NM, Pecci R, Bedini R, Pameijer CH, Somma F (2006) Three-dimensional imaging using microcomputed tomography for studying tooth macromorphology. *J Am Dent Assoc* 137: 1555–1561. PMID: [17082282](#)

41. Grine FE (2004) Geographic variation in tooth enamel thickness does not support Neandertal involvement in the ancestry of modern Europeans. *S Afr J Sci* 100: 389–399.
42. Olejniczak AJ, Grine FE (2005) High resolution measurement of Neandertal tooth enamel thickness by micro focal computed tomography. *S Afr J Sci* 101: 219–220.
43. Badawi-Fayad J, Yazbeck C, Balzeau A, Nguyen T, Istoc A, Grimaud-Hervé D, Cabanis E (2005) Multi detector row CT scanning in paleoanthropology at various tube current settings and scanning modes. *Surgical and Radiologic Anatomy* 27: 536–543. PMID: [16211320](#)
44. Balzeau A, Crevecoeur I, Rougier H, Froment A, Gilissen E, Grimaud-Hervé D, et al (2010) Applications of imaging methodologies to Paleoanthropology: Beneficial results relating to the preservation, management and development of collections. *C R Palevol* 9: 265–275. ééeé doi: [10.1016/j.crpv.2010.07.006](#)
45. Smilg JS (2010) Advances in CT scanning of fossil-bearing rocks from the Malapa site, South Africa (Oral presentation). Shanghai World Expo Seminar on Palaeontology.
46. Bollinger SA, Ross S, Thali MJ, Hostettler B, Menkveld-Gfeller U (2012) Scenes from the Past—initial investigation of early jurassic vertebrate fossils with multidetector CT. *Radiographics* 1553–1559. doi: [10.1148/rg.325115742](#) PMID: [22977034](#)
47. Rahman IA, Adcock K, Garwood R (2012) Virtual Fossils: a New Resource for Science Communication in Paleontology. *Evo Edu Outreach* 5: 635–641.
48. Carpenter K (2001) How to make a Fossil: Part 1—Fossilizing bone. *The Journal of Paleontological Sciences* 07: 1–10.
49. Croker SL, Clement JG, Donlon D (2009) A comparison of cortical bone thickness in the femoral mid-shaft of humans and two non-human mammals. *HOMO—Journal of Comparative Human Biology* 60: 551–565. doi: [10.1016/j.jchb.2009.07.003](#)
50. Ketcham RA, Carlson WD (2001) Acquisition, optimization and interpretation of X ray computed tomographic imaging: Application to the Geosciences. *Computers and Geosciences* 27: 381–400.
51. Zatz LM (1981) Basic principles of computed tomography. In: Newton TH, Potts DG, editors. *Technical aspects of Computed Tomography*. St. Louis: Mosby. pp. 385–387.
52. Kimpe T, Tuytschaever T (2007) Increasing the number of gray shades in medical display systems—how much is enough? *J Digit Imaging Dec*: 422–432.
53. Adcock D (2002) Digital imaging.
54. Zollikofer C. and Ponce de Leon M. S. (2005) *Virtual reconstruction: a primer in computer assisted paleontology and biomedicine*. New York: John Wiley & Sons.
55. Weber G. W. and Bookstein F. L. (2011) *Virtual Anthropology- A guide to a new interdisciplinary field*. SpringerWein NewYork.
56. Barret JF, Keat N (2004) Artifact in CT: Recognition and Avoidance. *Radiographics* 24: 1679–1691. PMID: [15537976](#)
57. Willis PMA, Robinson J, Kemp A (1995) Computerised tomographic scans of an Eocene crocodile skull from Southeast Queensland. *Mem Ass Australas Palaeontol* 18: 203–208.
58. Peyton RL, Haeffner BA, Anderson SH, Gantzer CJ (1992) Applying X- ray CT to measure macropore diameters in undisturbed soil cores. *Geoderma* 53: 329–340.
59. Spoor F, Zonneveld F (1994) The Bony Labyrinth in *Homo erectus*: a preliminary report. *Cour Firsch Inst Senchenberg* 171: 251–256.
60. Schoenemann PT, Gee J, Avants B, Holloway RL, Monge J, Lewis J (2007) Validation of plaster endocast morphology through 3D CT image analysis. *American Journal of Physical Anthropology* 132: 183–192. PMID: [17103425](#)
61. Richtsmeier JT, Paik CH, Elfert PC, Cole TM, Dahlman HR (1995) Precision repeatability and validation of the localization of cranial landmarks using computed tomography scans. *Cleft Palate Craniofac J* 32: 217–227. PMID: [7605789](#)
62. Coleman MN, Colbert MW (2007) Technical note: CT thresholding protocols for taking measurement on three-dimensional models. *American Journal of Physical Anthropology* 133: 723–725. PMID: [17326102](#)
63. Hoffman R, Schultz JA, Schellhorn R, Rybachi E, Keupp H, Gerden SR, et al (2014) Non-invasive imaging methods applied to neo-and paleo-ontological cephalopod research. *Biogeosciences* 11: 2721–2739.